

Discovery of a double detonation thermonuclear supernova progenitor

THOMAS KUPFER,¹ EVAN B. BAUER,² JAN VAN ROESTEL,³ ERIC C. BELLM,⁴ LARS BILDSTEN,^{5,6} JIM FULLER,³
THOMAS A. PRINCE,³ ULRICH HEBER,⁷ STEPHAN GEIER,⁸ MATTHEW J. GREEN,⁹ SHRINIVAS R. KULKARNI,³
STEVEN BLOEMEN,¹⁰ RUSS R. LAHER,¹¹ BEN RUSHOLME,¹¹ AND DAVID SCHNEIDER⁷

¹*Department of Physics and Astronomy, Texas Tech University, PO Box 41051, Lubbock, TX 79409, USA*

²*Center for Astrophysics | Harvard & Smithsonian, 60 Garden St, Cambridge, MA 02138, USA*

³*Division of Physics, Mathematics and Astronomy, California Institute of Technology, Pasadena, CA 91125, USA*

⁴*DIRAC Institute, Department of Astronomy, University of Washington, 3910 15th Avenue NE, Seattle, WA 98195, USA*

⁵*Kavli Institute for Theoretical Physics, University of California, Santa Barbara, CA 93106, USA*

⁶*Department of Physics, University of California, Santa Barbara, CA 93106, USA*

⁷*Dr. Karl Remeis-Observatory & ECAP, Astronomical Institute, Friedrich-Alexander University Erlangen-Nuremberg (FAU), Sternwartstr. 7, 96049 Bamberg, Germany*

⁸*Institut für Physik und Astronomie, Universität Potsdam, Haus 28, Karl-Liebknecht-Str. 24/25, D-14476 Potsdam-Golm, Germany*

⁹*Department of Astrophysics, School of Physics and Astronomy, Tel Aviv University, Tel Aviv 6997801, Israel*

¹⁰*Department of Astrophysics/IMAPP, Radboud University Nijmegen, P.O. Box 9010, 6500 GL Nijmegen, The Netherlands*

¹¹*IPAC, California Institute of Technology, 1200 E. California Blvd, Pasadena, CA 91125, USA*

(Received June 1, 2019; Revised January 10, 2019; Accepted January 7, 2022)

Submitted to ApJL

ABSTRACT

We present the discovery of a new double detonation progenitor system consisting of a hot subdwarf B (sdB) binary with a white dwarf companion with an $P_{\text{orb}}=76.34179(2)$ min orbital period. Spectroscopic observations are consistent with an sdB star during helium core burning residing on the extreme horizontal branch. Chimera light curves are dominated by ellipsoidal deformation of the sdB star and a weak eclipse of the companion white dwarf. Combining spectroscopic and light curve fits we find a low mass sdB star, $M_{\text{sdB}} = 0.383 \pm 0.028 M_{\odot}$ with a massive white dwarf companion, $M_{\text{WD}} = 0.725 \pm 0.026 M_{\odot}$. From the eclipses we find a blackbody temperature for the white dwarf of 26,800 K resulting in a cooling age of ≈ 25 Myrs whereas our MESA model predicts an sdB age of ≈ 170 Myrs. We conclude that the sdB formed first through stable mass transfer followed by a common envelope which led to the formation of the white dwarf companion ≈ 25 Myrs ago.

Using the MESA stellar evolutionary code we find that the sdB star will start mass transfer in ≈ 6 Myrs and in ≈ 60 Myrs the white dwarf will reach a total mass of $0.92 M_{\odot}$ with a thick helium layer of $0.17 M_{\odot}$. This will lead to a detonation that will likely destroy the white dwarf in a peculiar thermonuclear supernova. PTF1 J2238+7430 is only the second confirmed candidate for a double detonation thermonuclear supernova. Using both systems we estimate that at least $\approx 1\%$ of white dwarf thermonuclear supernovae originate from sdB+WD binaries with thick helium layers, consistent with the small number of observed peculiar thermonuclear explosions.

Keywords: Eclipsing binary stars(444) — White dwarf stars(1799) — Close binary stars(254) — B subdwarf stars(129)

1. INTRODUCTION

Most hot subdwarf B stars (sdBs) are core helium burning stars with masses around $0.5 M_{\odot}$ and thin hydrogen envelopes (Heber 1986, 2009, 2016). A large number of sdB stars are in close orbits with orbital periods of $P_{\text{orb}} < 10$ days (Napiwotzki et al. 2004; Maxted et al. 2001), with the most compact systems reaching orbital periods of $\lesssim 1$ hour (e.g. Vennes et al. 2012; Geier et al. 2013; Kupfer et al. 2017a,b, 2020a,b). The only way to form such tight binaries is orbital shrinkage through a common envelope phase followed by the loss of angular momentum due to the radiation of gravitational waves (Han et al. 2002, 2003; Nelemans 2010).

SdB binaries with white dwarf (WD) companions which exit the common envelope phase at $P_{\text{orb}} \lesssim 2$ hours will reach contact while the sdB is still burning helium (Bauer & Kupfer 2021). Due to the emission of gravitational waves the orbit of the binary will shrink until the sdB fills its Roche Lobe at a period of $\approx 30 - 100$ min, depending on the evolutionary stage and envelope thickness of the hot subdwarf (e.g. Savonije et al. 1986; Tutukov & Fedorova 1989; Tutukov & Yungelson 1990; Iben & Tutukov 1991; Yungelson 2008; Piersanti et al. 2014; Brooks et al. 2015; Neunteufel et al. 2019; Bauer & Kupfer 2021).

The known population of sdB + WD binaries consists mostly of systems with orbital periods too large to start accretion before the sdB turns into a WD (Kupfer et al. 2015). Currently only four detached systems with a WD companion are known to have $P_{\text{orb}} < 2$ hours (Vennes et al. 2012; Geier et al. 2013; Kupfer et al. 2017a,b; Pelisoli et al. 2021). Just recently Kupfer et al. (2020a,b) discovered the first two Roche lobe filling hot subdwarfs as part of a high-cadence Galactic Plane survey using the Zwicky Transient Facility (Kupfer et al. 2021). Both systems can be best explained as Roche Lobe filling sdOB stars which have started mass transfer to a WD companion. The light curves in both systems show deep eclipses from an accretion disk. Due to their high effective temperatures, both sdOB stars are predicted to be in a short lived phase where the sdOB undergoes residual hydrogen shell burning.

The most compact known sdB binary where the sdB is still undergoing core-helium burning is CD-30°11223. The binary has an orbital period $P_{\text{orb}} = 70.5$ min and a high mass WD companion ($M_{\text{WD}} \approx 0.75 M_{\odot}$; Vennes et al. 2012; Geier et al. 2013). The sdB in CD-30°11223 will begin transferring helium to its WD companion in ≈ 40 Myr when the system has shrunk to an orbital period $P_{\text{orb}} \approx 40$ min. After the WD accretes $\approx 0.1 M_{\odot}$, helium burning is predicted to be ignited unstably in the accreted helium layer on the WD surface (Brooks et al. 2015; Bauer et al. 2017). This could either disrupt the WD even when the mass is significantly below the Chandrasekhar mass, a so-called double detonation supernova (e.g. Livne 1990; Livne & Arnett 1995; Fink et al. 2010; Woosley & Kasen 2011; Wang & Han 2012; Shen & Bildsten 2014; Wang 2018) or just detonate the He-shell without disrupting the WD which results in a faint and fast .Ia supernova with subsequent weaker He-flashes (Bildsten et al. 2007; Brooks et al. 2015). Therefore, systems like CD-30°11223 are predicted to be either the progenitors for double detonation thermonuclear supernovae or perhaps faint and fast .Ia supernovae that do not disrupt the WD.

De et al. (2019, 2020) presented the discovery of a sample of calcium-rich transients consistent with a thick helium shell double detonation on a sub-Chandrasekhar-mass WD (Polin et al. 2019, 2021). The majority of these transients are located in old stellar populations with only a small sub-sample found in in star forming environments.

The question remains just how common systems like CD-30°11223 are. To address this question we have conducted a search for (ultra-)compact post-common envelope systems using the Palomar Transient Factory (PTF; Law et al. 2009; Rau et al. 2009) and subsequently the Zwicky Transient Facility (ZTF; Graham et al. 2019; Masci et al. 2019) based on a color selected sample from Pan-STARRS data release 1. The PTF used the Palomar 48" Samuel Oschin Schmidt telescope to image up to $\approx 2000 \text{ deg}^2$ of the sky per night to a depth of $R_{\text{mould}} \approx 20.6 \text{ mag}$ or $g' \approx 21.3 \text{ mag}$. PTF was succeeded by the Zwicky Transient Facility which started science operation in March 2018 using the same telescope but a new camera with a field-of-view of 47 deg^2 . Here we report the discovery of a new thermonuclear supernova double detonation progenitor system consisting of an sdB with a WD companion: PTF1 J223857.11+743015.1 (hereafter PTF1 J2238+7430) with orbital period of 76 min showing similar properties to CD-30°11223.

2. OBSERVATIONS

2.1. Photometry

As part of the Palomar Transient Factory (PTF), the Palomar 48-inch (P48) telescope imaged the sky every night. The reduction pipeline for PTF applies standard de-biasing, flat-fielding, and astrometric calibration to raw images (Laher et al. 2014). Relative photometry correction is applied and absolute photometric calibration to the few percent level is performed using a fit to SDSS fields observed in the same night (Ofek et al. 2012). The lightcurve of PTF1 J2238+7430 has 144 epochs, with good photometry in the R_{mould} band with a typical uncertainty of 0.01-0.02 mag. The majority of observations were conducted during the summer months June - August 2013 and 2014 and

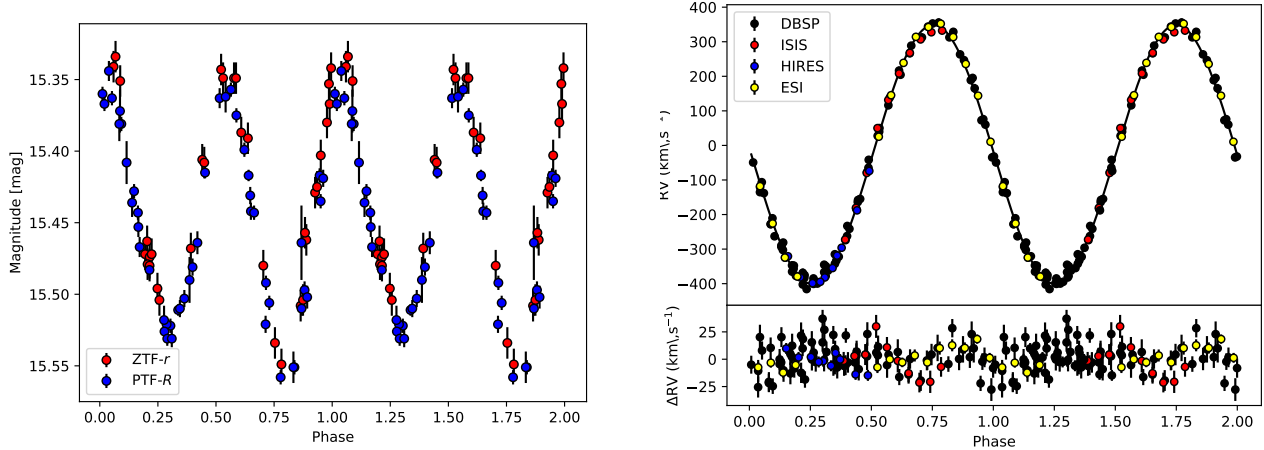


Figure 1. Left panel: Phase folded at $P_{\text{orb}}=76.341750$ min ZTF and PTF light curve for PTF1 J2238+7430. **Right panel:** Radial velocity plotted against orbital phase for PTF1 J2238+7430. The RV data were phase folded with the orbital period and are plotted twice for better visualization. The residuals are plotted below.

the cadence is highly irregular, ranging from a few minutes to years. The object was also observed as part of the Zwicky Transient Facility (ZTF) public survey (Graham et al. 2019; Bellm et al. 2019). Image processing of ZTF data is described in full detail in Masci et al. (2019). We extracted the light curve from ZTF data release 6 which consists of 34 observations in ZTF- r taken randomly over ≈ 1.5 years between August 2018 and November 2019.

High-cadence observations were conducted using the Palomar 200-inch telescope with the high-speed photometer CHIMERA (Harding et al. 2016) which is a 2-band photometer which uses frame-transfer, electron-multiplying CCDs to achieve 15 ms dead time covering a 5×5 arcmin field of view. Simultaneous optical imaging in two bands is enabled by a dichroic beam splitter centered at 567 nm. Data reduction was carried out with the ULTRACAM pipeline (Dhillon et al. 2007) customized for CHIMERA. All frames were bias-subtracted and flat-fielded. 1300 observations in g' and r' with a 5 sec exposure time were obtained on 2017-07-26 and 2700 observations in g' and i' with a 4 sec exposure time were obtained on 2017-12-14.

2.2. Spectroscopy

Optical spectra were obtained with the Palomar 200-inch telescope and the Double-Beam Spectrograph (DBSP; Oke & Gunn 1982) using a low resolution mode ($R \sim 1500$). 31 consecutive exposures were obtained on 2017-05-25 and 2017-05-29 and 15 consecutive exposures were obtained on 2017-05-25 using a 180 sec exposure time. Each night an average bias and normalized flat-field frame was made out of 10 individual bias and 10 individual lamp flat-fields. To account for telescope flexure, an arc lamp was taken at the position of the target after each observing sequence. For the blue arm, FeAr and for the red arm, HeNeAr arc exposures were taken. Both arms of the spectrograph were reduced using a custom PyRAF-based pipeline¹(Bellm & Sesar 2016). The pipeline performs standard image processing and spectral reduction procedures, including bias subtraction, flat-field correction, wavelength calibration, optimal spectral extraction, and flux calibration.

Additionally PTF1 J2238+7430 was also observed with the William Herschel Telescope (WHT) and the ISIS spectrograph (Carter et al. 1993) using a medium resolution mode (R600B grating, $R \approx 2500$). 10 consecutive exposures with an exposure time of 180 sec were obtained on 2017-07-26. 10 bias frames were obtained to construct an average bias frame and 10 individual lamp flat-fields were obtained to construct a normalized flat-field. CuNeAr arc exposures were taken before and after the observing sequence to correct for instrumental flexure. One dimensional spectra were extracted using optimal extraction and were subsequently wavelength and flux calibrated.

To obtain high-resolution spectra, PTF1 J2238+7430 was observed with Keck/HIRES and Keck/ESI. We obtained 5 consecutive exposures with Keck/HIRES on 2017-08-14 and 2017-08-30 as well as 14 consecutive exposures with

¹ <https://github.com/ebellm/pyraf-dbsp>

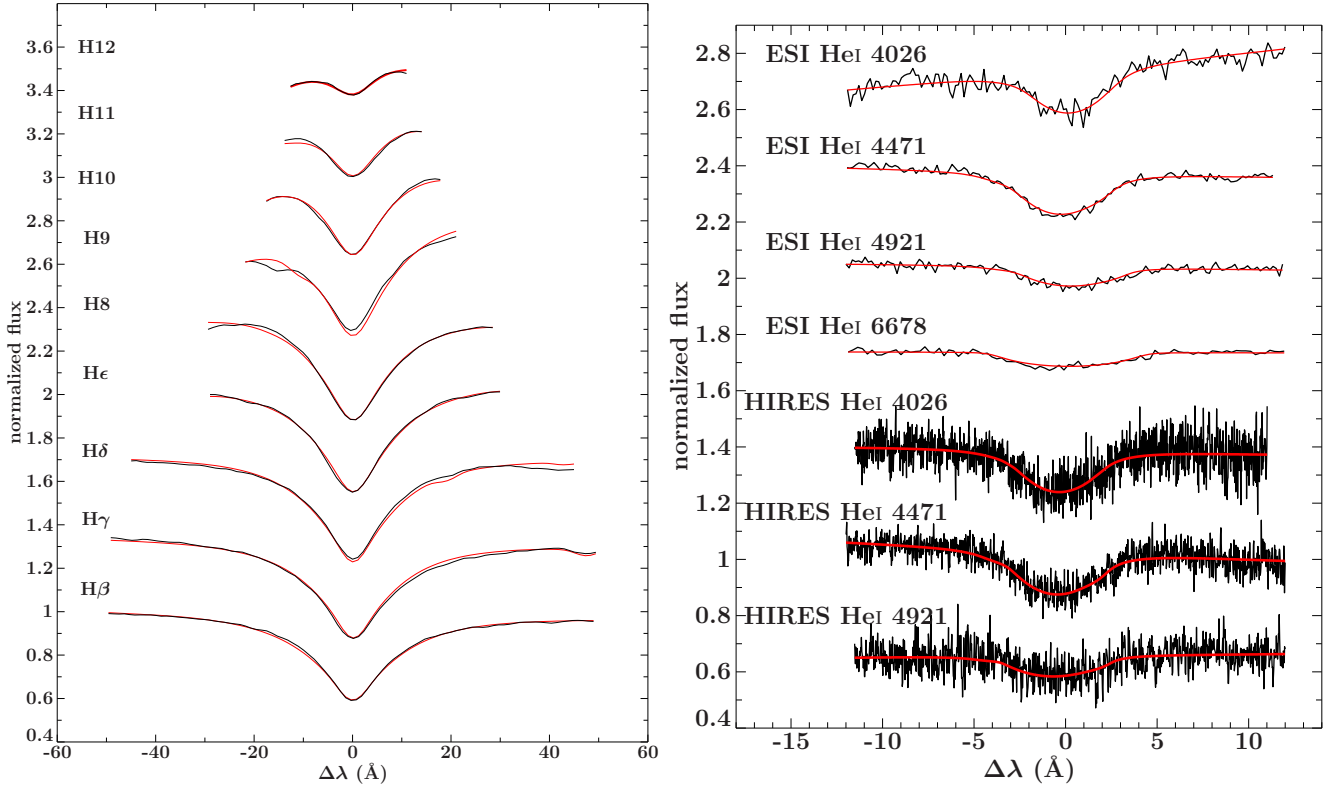


Figure 2. **Left panel:** Fit of synthetic LTE models to the hydrogen Balmer lines of a coadded DBSP spectrum. The normalized fluxes of the single lines are shifted for better visualisation. **Right panel:** Fits of $v_{\text{rot}} \sin i$ to the helium lines seen in the HIRES and ESI spectra. The atmospheric parameters were fixed to the values derived from the WHT and DBSP spectra.

Keck/ESI on 2018-07-20. ThAr arc exposures were taken at the beginning of the night. The spectra were reduced using the MAKEE² pipeline following the standard procedure: bias subtraction, flat fielding, sky subtraction, order extraction, and wavelength calibration.

3. ORBITAL AND ATMOSPHERIC PARAMETERS AND LIGHT CURVE FITTING

As evident in Fig. 1 PTF1 J2238+7430 shows strong periodic ellipsoidal variability in its light curve at $P_{\text{orb}} = 76.341750(1)$ min. This variability is caused by the tidal deformation of the sdB primary under the influence of the gravitational force of the companion. We use the PTF and the ZTF lightcurve with its multi-year baseline and the Chimera light curves to derive the orbital period of the systems. The analysis was done with the *Gatspy* module for time series analysis which uses the Lomb-Scargle periodogram³ (VanderPlas & Ivezić 2015). The error was derived from bootstrapping.

Radial velocities were measured by fitting Gaussians, Lorentzians, and polynomials to the hydrogen and helium lines to cover continuum, line, and line core of the individual lines using the FITSB2 routine (Napiwotzki et al. 2004). The procedure is described in full detail in Geier et al. (2011). We fitted the wavelength shifts compared to the rest wavelengths using a χ^2 -minimization. Assuming circular orbits, a sine curve was fitted to the folded radial velocity (RV) data points (Fig. 1).

Atmospheric parameters such as effective temperature, T_{eff} , surface gravity, $\log g$, helium abundance, $\log y = \log \frac{n(\text{He})}{n(\text{H})}$, and projected rotational velocity, $v_{\text{rot}} \sin i$, were determined by fitting the rest-wavelength corrected average DBSP, ISIS and HIRES spectra with metal-line-blanketed LTE model spectra (Heber et al. 2000). T_{eff} and $\log g$ were derived from the Balmer and helium lines from the ISIS and DBSP spectra whereas $\log y$ and $v_{\text{rot}} \sin i$ were measured with the HIRES spectra. High-resolution echelle spectra are not well suited to measure T_{eff} and $\log g$ because

² <https://sites.astro.caltech.edu/~tb/makee/>

³ <http://dx.doi.org/10.5281/zenodo.14833>

Table 1. Overview of the measured and derived parameters for PTF1 J2238+7430

Right ascension	RA [hrs]	22:38:57.11
Declination	Dec [°]	+74:30:15.1
Magnitude ^b	g [mag]	15.244±0.023
Parallax ^a	ϖ [mas]	1.0001 ± 0.0225
Distance	d [kpc]	1.00 ± 0.03
Absolute Magnitude (reddening corrected)	M_g [mag]	4.40 ± 0.20
Proper motion ^a (RA)	$\mu_\alpha \cos(\delta)$ [mas yr ⁻¹]	0.344 ± 0.056
Proper motion ^a (Dec)	μ_δ [mas yr ⁻¹]	-1.833 ± 0.051
Atmospheric parameters of the sdB		
Effective temperature ^c	T_{eff} [K]	23 600±400
Surface gravity ^c	$\log g$	5.42±0.06
Helium abundance ^d	$\log y$	-2.11±0.03
Projected rotational velocity ^d	$v_{\text{rot}} \sin i$ [km s ⁻¹]	185±5
Orbital parameters		
	T_0 [BJD UTC]	57960.47584170(3)
Orbital period	P_{orb} [min]	76.341750(1)
RV semi-amplitude	K [km s ⁻¹]	378.0 ± 3.7
System velocity	γ [km s ⁻¹]	-6.2 ± 2.14
Binary mass function	f_m [M _⊙]	0.0597±0.0020
Derived parameters		
Mass ratio	$q = \frac{M_{\text{WD}}}{M_{\text{sdB}}}$	0.528 ± 0.020
sdB mass	M_{sdB} [M _⊙]	0.383 ± 0.028
sdB radius	R_{sdB} [R _⊙]	0.190 ± 0.003
WD mass	M_{WD} [M _⊙]	0.725 ± 0.026
WD radius	R_{WD} [M _⊙]	0.0109 ^{+0.0002} _{-0.0003}
WD blackbody temperature	T_{eff} [K]	26,800 ± 4600
Orbital inclination	i [°]	88.4 ^{+1.6} _{-3.3}
Separation	a [R _⊙]	0.615 ± 0.010
Roche filling factor	$R_{\text{sdB}}/R_{\text{Roche lobe}}$	0.951 ± 0.010

^a from Gaia eDR3 (Gaia Collaboration et al. 2016, 2021)^b from PanSTARRS DR1 (Chambers et al. 2016)^c adopted from DBSP and ISIS^d adopted from ESI and HIRES

the broad hydrogen absorption lines span several individual echelle orders and merging of the echelle spectra could introduce systematic errors. The full procedure is described in detail in Kupfer et al. (2017a,b). PTF1 J2238+7430 shows typical T_{eff} , $\log g$, and $\log y$ and $v_{\text{rot}} \sin i = 185 \pm 5 \text{ km s}^{-1}$. The rotational velocity is consistent with a tidally locked sdOB star (see Sec. 4.1). Figure 2 shows the main Balmer and helium lines with the best fit to the data. Table 1 summarizes the atmospheric and orbital parameters.

To model the lightcurves obtained with CHIMERA we used the LCURVE code (Copperwheat et al. 2010). We use a Roche geometry, and the free parameters in our fit are: the phase (t_0), the scaled radii ($r_{1,2}$), the mass ratio q , the inclination i , secondary temperature T_{WD} , and the velocity scale ($[K + K_{\text{WD}}]/\sin i$). We use a passband-dependent gravity-darkening law and use a gravity darkening value ($y_{g,r}$) from Claret & Bloemen (2011) and find $\beta = 0.425$ for g' , $\beta = 0.395$ for r' , and $\beta = 0.37$ for i' . We assume an uncertainty of 0.03 on the value and use a Gaussian prior. We use fixed limb darkening coefficients (a_1, a_2, a_3, a_4) taken from Claret & Bloemen (2011). We use $a_1 = 0.82, a_2 = -0.65, a_3 = 0.55$, and $a_4 = -0.19$ for g' , $a_1 = 0.81, a_2 = -0.89, a_3 = 0.79$, and $a_4 = -0.27$ for r' , and $a_1 = 0.78, a_2 = -1.01, a_3 = 0.91$, and $a_4 = -0.31$ for i' . We also model the relativistic beaming (F) as

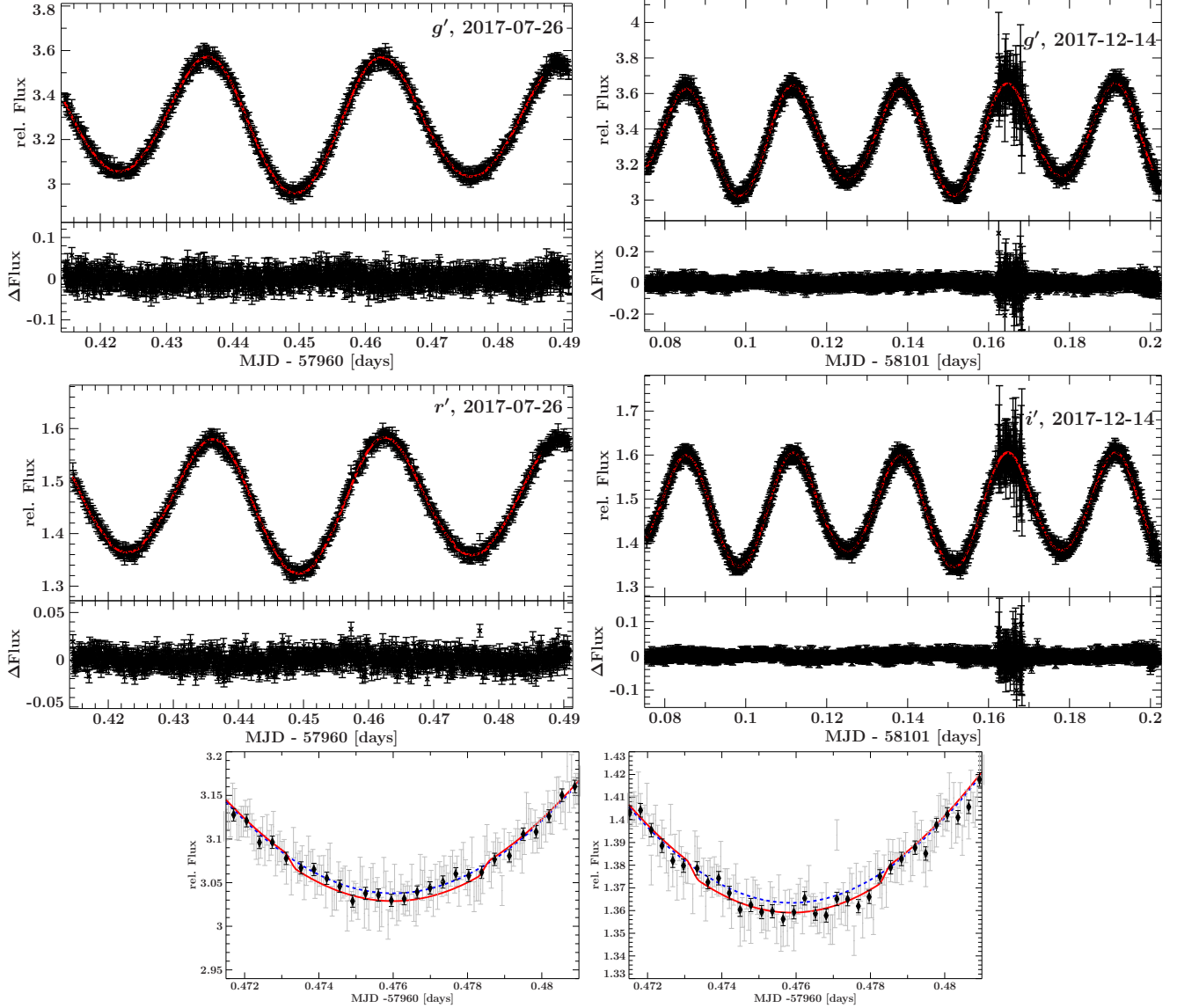


Figure 3. Chimera light curves un-binned (grey) and binned (black) shown together with the LCURVE fits (red) observed optical SDSS bandpasses. The lower two panels show the region when the WD is being eclipsed by the sdB. The blue solid curve marks the same model without eclipses of the WD. The lower panels show the region when the white dwarf is being eclipsed. **Lower left panel:** g' light curve, **Lower right panel:** r' light curve

in Bloemen et al. (2011). We calculate the beaming parameters by assuming a blackbody spectrum and using the effective wavelength of the g' , r' , and i' filters. We find $F = 1.80$ for g' , $F = 1.57$ for r' , and $F = 1.46$ for i' . The full approach is also described in Kupfer et al. (2017a,b, 2020a,b) and Ratzloff et al. (2019). In addition, we add a 2nd order polynomial to correct for any long timescale trends which are the result of a changing airmass over the course of the observations. The best value of χ^2 for this model was 1350 for 1300 data points for the g-band light curve which includes also a weak eclipse of the hot WD. Although the eclipse is weak ($\leq 1\%$; Fig. 3), the χ^2 for the non-eclipsing solution is 1400 which is statistically significantly worse compared to the solution with the weak eclipse. We use the MCMC sampler EMCEE (Foreman-Mackey et al. 2013) to determine the best-fit values and uncertainty on the parameters. Figure 3 shows the Chimera light curves with the best fitted model. The lower panels are zoomed in around the region when the WD is being eclipsed.

4. RESULTS

4.1. System parameters

Although, PTF1 J2238+7430 is a single-lined binary we can derive system parameters using the combined results from the light curve analysis with results from the spectroscopic fitting. Parameters derived in this way by a simultaneous fit to the Chimera light curves are summarized in Table 1. The given errors are all 95 % confidence limits.

We find that PTF1 J2238+7430 consists of a low mass sdB with a high-mass WD companion. We derive a mass ratio $q = M_{\text{sdb}}/M_{\text{WD}} = 0.528 \pm 0.020$, a mass for the sdB $M_{\text{sdb}} = 0.383 \pm 0.028 M_{\odot}$, and a WD companion mass $M_{\text{WD}} = 0.725 \pm 0.026 M_{\odot}$. PTF1 J2238+7430 is found to be eclipsing at an inclination angle of $i = 88.4_{-3.3}^{+1.6}^{\circ}$ which allows us to measure the radius and the black-body temperature of the WD companion. We determine a black-body temperature of $26,800 \pm 4600$ K for the WD and a radius of $R_{\text{WD}} = 0.0109_{-0.0003}^{+0.0002} R_{\odot}$. The radius was found to be $< 5\%$ above the zero-temperature value and is fully consistent with predictions from Romero et al. (2019) for carbon-oxygen core white dwarfs.

Zahn (1977) predicted that the sdBs in close sdB binaries with orbital periods below ≈ 0.3 days should be synchronized to the orbit. More recently, Preece et al. (2018) found that only the most compact sdB binaries should be synchronized. From the system parameters we find that the sdB would have a projected rotational velocity $v_{\text{rot}} \sin i = 181 \pm 6 \text{ km s}^{-1}$ if synchronized to the orbit. The measured $v_{\text{rot}} \sin i = 185 \pm 5 \text{ km s}^{-1}$ is consistent with a synchronized orbit.

We calculate the absolute magnitude (M_g) of PTF1 J2238+7430 using the visual PanSTARRS g-band magnitude $g = 15.244 \pm 0.023 \text{ mag}$ and the parallax from Gaia eDR3 (Gaia Collaboration et al. 2016, 2021). Because the object is located near the Galactic Plane, significant reddening can occur. Green et al. (2019) present updated 3D extinction maps based on Gaia parallaxes and stellar photometry from Pan-STARRS 1 and 2MASS⁴ and find towards the direction of PTF1 J2238+7430 an extinction of $E(g-r) = 0.24 \pm 0.03$ at a distance of 1.00 kpc; this results in a total extinction in the g-band of $A_g = 0.84 \pm 0.11 \text{ mag}$, and with the corrected magnitude, we find an absolute magnitude of $M_g = 4.40 \pm 0.20 \text{ mag}$ consistent with a hot subdwarf star (Geier et al. 2019).

4.2. Comparison with Gaia parallax

To test whether our derived system parameters are consistent with the parallax provided by Gaia eDR3, we compared the measured parameters from the light curve fit to the predictions using the Gaia parallax. The approach follows a similar strategy as described in Ratzloff et al. (2019) and Kupfer et al. (2020a). Using the absolute magnitude $M_g = 4.40 \pm 0.20 \text{ mag}$, we find a luminosity of $L = 11.5 \pm 3.0 L_{\odot}$ using a bolometric correction $BC_g = -2.30 \text{ mag}$ derived for our stellar parameters from the MESA Isochrones & Stellar Tracks (MIST; Dotter 2016; Choi et al. 2016; Paxton et al. 2011, 2013, 2015, 2018). Using the Stefan-Boltzmann law applied to a black body ($L = 4\sigma\pi R_{\text{sdb}}^2 T_{\text{eff}}^4$), we can solve for the radius of the sdBs, and combined with $R_{\text{sdb}}^2 = GM_{\text{sdb}}/g$, we can solve for mass of the sdBs:

$$M_{\text{sdb}} = \frac{L_{\text{sdb}} 10^{\log(g)}}{4\pi\sigma G T_{\text{eff}}^4} \quad (1)$$

Using these equations we find $M_{\text{sdb}} = 0.39 \pm 0.10 M_{\odot}$ and $R_{\text{sdb}} = 0.17 \pm 0.03 R_{\odot}$. Although the error bars are rather large, this result is in agreement with the results from the light curve and spectroscopic fits.

4.3. Kinematics of the binary systems

We find that PTF1 J2238+7430 has evolved from a $\approx 2 M_{\odot}$ star (see Sect. 5.2), and we expect the system is a member of a young stellar population. Using the proper motion from Gaia eDR3 (Gaia Collaboration et al. 2016, 2018, 2021), the distance and the systemic velocities (see Tab. 1) we calculate the Galactic motion for PTF1 J2238+7430.

We employed the approach described in Odenkirchen & Brosche (1992) and Pauli et al. (2006). As in Kupfer et al. (2020a), we use the Galactic potential of Allen & Santillan (1991) as revised by Irrgang et al. (2013). The orbit was integrated from the present to 3 Gyr into the past. We find that the binary moves within a height of 200 parsec of the Galactic equator and with very little eccentricity between 9 and 10 kpc from the Galactic center. From the Galactic orbit we conclude that PTF1 J2238+7430 is a member of the Galactic thin disk population consistent with being member of a young stellar population.

⁴ <http://argonaut.skymaps.info/>

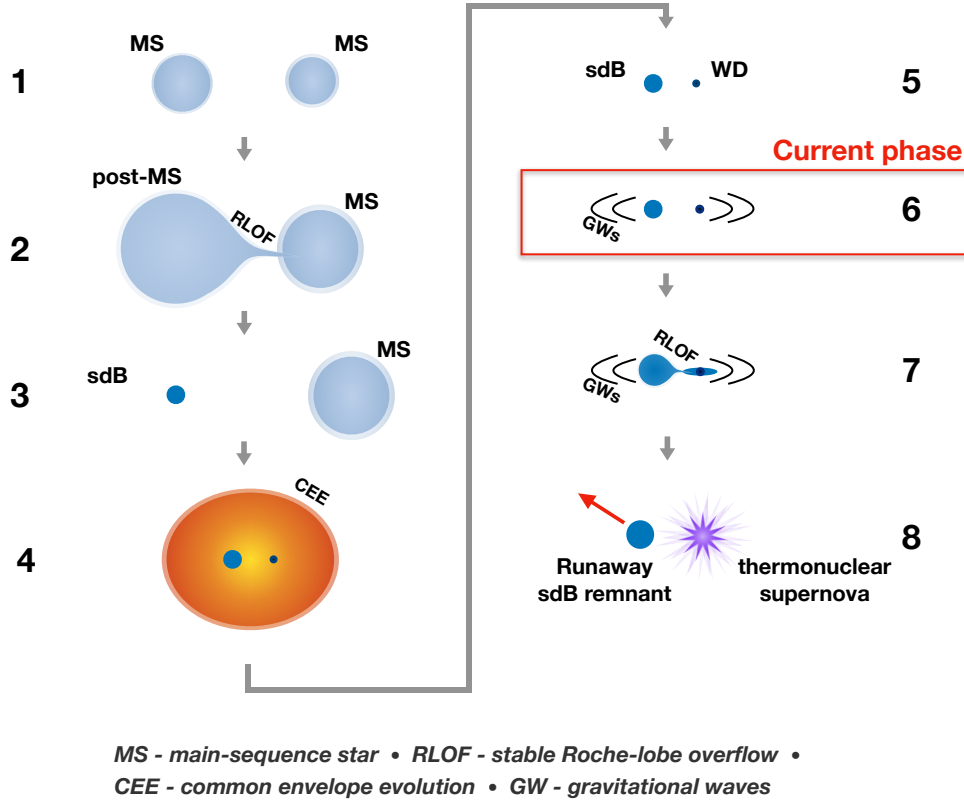


Figure 4. Visualization of the proposed evolutionary pathway for PTF1 J2238+7430. The red box marks the current evolutionary phase. Each evolutionary phase is numbered according to their order in the evolution and the direction of the sequence is marked with arrows.

5. PREDICTED EVOLUTION OF THE BINARY SYSTEM

5.1. Formation of the sdB + WD system

Ruiter et al. (2010) found that the dominant way to form compact double carbon-oxygen core WDs is through stable mass transfer which forms the sdB followed by a phase of unstable mass transfer which forms the white dwarf companion. They present a specific example which starts with a $2.88 M_{\odot}$ and $2.45 M_{\odot}$ binary pair. In PTF1 J2238+7430 weak eclipses of the WD companion imply a blackbody temperature of $26\,800 \pm 4600$ K. From the blackbody temperature we can estimate the cooling age and find a cooling time of ≈ 25 million years, significantly shorter than the predicted current age of the sdB of ≈ 170 million years (see Sec. 5.2). Therefore, we predict that the sdB was formed first, and we propose the following evolutionary scenario (illustrated in Fig. 4) for PTF1 J2238+7430 which explains all observational properties and is similar to the scenario discussed in Ruiter et al. (2010).

The system started as a $\approx 2 M_{\odot}$ main sequence star (see Sect. 5.2) which will become the sdB, and a slightly lower mass companion with an orbital period of a few weeks. The sdB progenitor evolves first and starts stable mass transfer to the companion star. At the end of that phase the sdB has formed with the observed mass of $\approx 0.4 M_{\odot}$ and the orbital periods has substantially widened consistent with the first stable RLOF channel described in Han et al. (2002, 2003). The companion star has accreted $\approx 1.7 M_{\odot}$ of material from the sdB progenitor and turned into a $\approx 3.5\text{--}4 M_{\odot}$ star which will then evolve off the main sequence and overflow its Roche Lobe while the sdB star is still burning helium. Due to the large mass ratio at this point, mass transfer will be unstable and initiate a common envelope. The CE phase could happen either during the RGB or AGB phase of the secondary depending on the binary separation at that point. In either case it would leave a compact binary with a massive WD and an sdB at an orbital period of ≈ 86 minutes. The observed high WD mass of $0.725 \pm 0.026 M_{\odot}$ is consistent with the evolution from an intermediate mass main

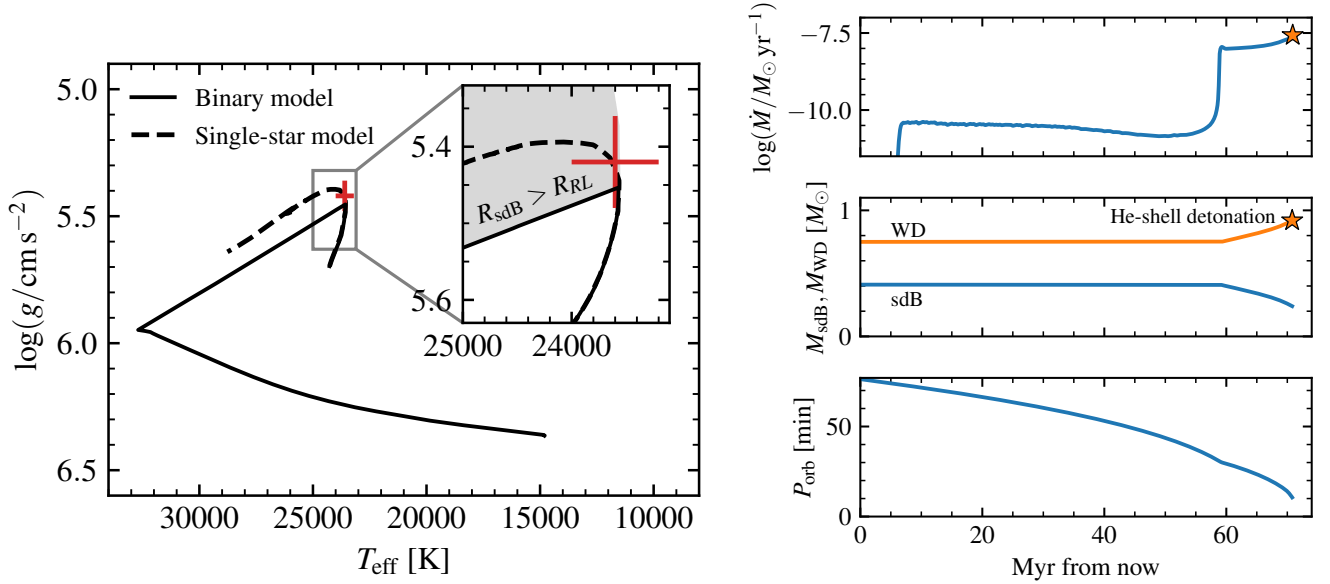


Figure 5. Left panel: Predicted evolution based on the MESA model for the PTF1 J2238+7430 system. The current observed $\log g$ and T_{eff} and error bars for the system are shown in red. The dashed curve shows the evolution the star would follow in isolation, while the solid curve shows the trajectory it follows due to encountering the Roche limit, depicted by the gray shaded region in the inset. **Right panel:** Future evolution of the system until the helium ignites.

sequence star (Cummings et al. 2018). The final phase of unstable mass transfer happened ≈ 25 million years ago, after which the WD cooled to its currently observed temperature while gravitational wave radiation decreased the orbital period to the currently observed period of 76 minutes. As also discussed in Ruiter et al. (2010), there could exist a substantial fraction of compact sdB+WD binaries where the sdB was formed first through stable mass transfer.

5.2. Future evolution

To understand the future evolution of the system we employed MESA version 12115 (Paxton et al. 2011, 2013, 2015, 2018, 2019). Bauer & Kupfer (2021) use MESA models to show that sdB stars with mass $M \lesssim 0.47 M_{\odot}$ can descend from either lower-mass main sequence progenitors that ignite central He burning via an off-center degenerate He flash ($M_{\text{ZAMS}} \lesssim 2.3 M_{\odot}$), or they can descend from higher-mass main sequence progenitors that ignite He at the center under non-degenerate conditions ($M_{\text{ZAMS}} \gtrsim 2.3 M_{\odot}$).⁵ They show that these scenarios lead to different H envelope structures that influence the subsequent radius evolution of the sdB star, with stars descended from higher mass progenitors having more compact envelopes and correspondingly higher $\log g$ values, as shown in the top panels of figure 5 in Bauer & Kupfer (2021). The measured $\log g$ for PTF1 J2238+7430 requires a relatively extended envelope with a radius that requires that the sdB star descended from the lower-mass channel with a progenitor mass around $2 M_{\odot}$. We find that our best matching MESA model for the measured $\log g$ and T_{eff} of this system is a $0.41 M_{\odot}$ sdB model descended from a $2.14 M_{\odot}$ main sequence star that ignited the He core via a degenerate He-core flash. This model has a sharp transition from the He core to an H envelope with solar composition. When He ignites, we remove most of the envelope, leaving a thin H envelope layer of $10^{-3} M_{\odot}$ so that the subsequent sdB evolution track matches the observed $\log g$ and T_{eff} of PTF1 J2238+7430. Figure 5 shows the $\log g$ – T_{eff} evolution of this MESA model, where it approaches the current observed state of PTF1 J2238+7430 after ≈ 170 Myr of evolution, and will encounter its Roche lobe and begin transferring mass soon after.

We model the future binary evolution of this system with a $0.75 M_{\odot}$ WD companion using the MESA binary capabilities. The WD model is constructed with a C/O core using the `make_co_wd` test case from MESA, rescaled to a mass of $0.75 M_{\odot}$, and cooled to the current observed temperature before initializing it into the MESA binary model at the currently observed orbital period with the sdB model. The sdB is currently observed at 95 % Roche Lobe filling and

⁵ The precise value of the progenitor M_{ZAMS} for which He ignition conditions change depends somewhat on metallicity and overshoot (Ostrowski et al. 2021), but generally lies between about 2.0 and $2.3 M_{\odot}$.

will continue to spiral in due to gravitational wave radiation. In our model the sdB will soon fill its Roche lobe and start to donate its hydrogen rich envelope in six million years at a low rate of $\lesssim 10^{-10} M_{\odot} \text{ yr}^{-1}$ (see [Bauer & Kupfer 2021](#), for a detailed overview). Because of the large initial radius of the H envelope, mass transfer will proceed at this low rate for ≈ 50 Myr before the H envelope is exhausted and the He core is finally exposed at a much more compact radius. While the sdB is still helium core burning ≈ 60 Myr from today, the sdB will begin to donate helium rich material onto the WD at the expected rate of $\approx 1\text{--}3 \times 10^{-8} M_{\odot} \text{ yr}^{-1}$, as shown in Figure 5. A helium rich layer will slowly build up for 10 million years, reaching a critical mass of $0.17 M_{\odot}$, after which the MESA WD model experiences He ignition in the accreted envelope. At this point the binary has an orbital period of ≈ 10 min. The sdB has been stripped down to a mass of $0.25 M_{\odot}$, and the WD has a total mass of $0.92 M_{\odot}$.

Our MESA model predicts that at this point the accreting WD will experience a thermonuclear instability that will lead to a detonation that will likely destroy the WD in a thermonuclear supernova ([Woosley & Kasen 2011](#); [Bauer et al. 2017](#)). Our MESA model for the WD accretor includes the NCO reaction chain as in [Bauer et al. \(2017\)](#), and this governs ignition in the accreted He envelope. Because this ignition mechanism is initiated by electron captures on ^{14}N , it occurs at a density above $\rho = 10^6 \text{ g cm}^{-3}$ where a detonation is likely to form ([Woosley & Weaver 1994](#); [Woosley & Kasen 2011](#)). The structure of our MESA model at the point of detonation is very similar to the model for CD-30°11223 in [Bauer et al. \(2017\)](#), which includes a more detailed discussion of detonation formation under these ignition conditions. At the time of the thermonuclear supernova, the sdB remnant has an orbital velocity of 911 km s^{-1} and will be released as a hyper-runaway star exceeding the escape velocity of the Galaxy ([Bauer et al. 2019](#); [Neunteufel 2020](#); [Neunteufel et al. 2021](#); [Liu et al. 2021](#)). Fig. 4 illustrates the evolutionary sequence proposed for PTF1 J2238+7430.

6. SUPERNOVA RATE ESTIMATE

Models of thermonuclear supernovae in WDs with thick ($\gtrsim 0.1 M_{\odot}$) helium shells indicate that they will yield transients classified as peculiar Type I supernovae ([Polin et al. 2019](#); [De et al. 2019](#)). PTF1 J2238+7430 together with CD-30°11223 therefore mark a small sample of double detonation peculiar thermonuclear supernova progenitors. Using both systems we can estimate a lower limit of thermonuclear supernovae originating in compact hot subdwarf + WD binaries where the sdB donates helium rich material during helium core burning. Both systems will have an age of ≈ 500 Myrs at the time of the helium shell detonation and are located within 1 kpc. Because of their young age, we compare the rate of these double detonation progenitors to the supernova Ia rate as a function of star formation. Under the assumption that these systems typically have an age of ≈ 500 Myrs at time of explosion we find a lower limit of double detonation explosions of $\frac{2}{500} \text{ kpc}^{-2} \text{ Myr}^{-1}$ from the two known systems. We can compare that to the local star formation rate of $10^{-3} M_{\odot} \text{ kpc}^{-2} \text{ yr}^{-1}$ which leads to a double detonation rate of $\approx 4 \times 10^{-6} \text{ yr}^{-1}$. [Sullivan et al. \(2006\)](#) found a supernova Ia rate of $3.9 \pm 0.7 \times 10^{-4} \text{ SNe yr}^{-1} (M_{\odot} \text{ yr}^{-1})^{-1}$ of star formation. With a Galactic star formation rate of $\approx 1 M_{\odot} \text{ yr}^{-1}$, we find that the rate at which peculiar thermonuclear supernovae with thick $\approx 0.15 M_{\odot}$ helium shells occur in star forming galaxies could be at least 1 % of the type Ia supernova rate. This is in reasonable agreement with the presently observed low rate of thick helium shell detonations. We note that thermonuclear supernovae with thick helium layers are likely to produce a transient that would be classified as a peculiar SN Ia with lower luminosities and redder color compared to ordinary SN Ia ([Polin et al. 2019](#)).

[De et al. \(2019\)](#) presented the discovery of peculiar Type I supernova consistent with a thick helium shell double detonation on a sub-Chandrasekhar-mass WD ([Polin et al. 2019, 2021](#)). However, one of the distinct differences is that the transient occurred in the outskirts of an elliptical galaxy which points to an old stellar population which is in disagreement with our observed systems which represent a young population. More recently, [De et al. \(2020\)](#) presented a sample of calcium rich transients originating from double-detonations with helium shells. They find that the majority of transients are located in old stellar populations. However, [De et al. \(2020\)](#) note that a small subsample (iPTF16hgs, SN2016hmk and SN 2019ofm) were found in star forming environments, suggesting that there is a small but likely non-zero contribution from young systems which could potentially be related to systems like CD-30°11223 and PTF1 J2238+7430.

7. SUMMARY AND CONCLUSION

As part of our search for short period sdB binaries we discovered PTF1 J2238+7430 using PTF and subsequently ZTF light curves. We find a period of $P_{\text{orb}} = 76.34179(2) \text{ min}$. Follow-up observations confirmed the system as an sdB with $M_{\text{sdB}} = 0.383 \pm 0.028 M_{\odot}$ and a WD companion with $M_{\text{WD}} = 0.725 \pm 0.026 M_{\odot}$. High-speed photometry observations with Chimera revealed a weak WD eclipse which allows us to measure the blackbody temperature and

radius of the WD. We find a temperature of $26,800 \pm 4600$ K and a radius of $R_{\text{WD}} = 0.0109^{+0.0002}_{-0.0003} R_{\odot}$ fully consistent with cooling models for carbon-oxygen core WDs. We find a cooling age of ≈ 25 Myrs for the WD which is significantly shorter than our age estimate for the sdB which is ≈ 170 Myrs. This can be explained by the sdB forming first through stable mass transfer, followed by the WD forming ≈ 25 Myrs ago through a common envelope phase. This shows that evolutionary scenarios where the sdB is formed first through stable mass transfer must be considered for compact sdB binaries with WD companions.

We employed MESA to calculate the future evolution of the system, finding that the sdB in PTF1 J2238+7430 will start mass transfer of the hydrogen rich envelope in ≈ 6 Myr. In ≈ 60 Myr, after a phase of hydrogen and helium mass transfer, the WD will build up a helium layer of $0.17 M_{\odot}$ leading to a total WD mass of $0.92 M_{\odot}$. Our models predict that at this point the WD will likely detonate in a peculiar thermonuclear supernova making PTF1 J2238+7430 the second known progenitor for a supernova with a thick helium layer. Using both systems we estimate that at least 1 % of type Ia supernova originate from compact sdB+WD binaries in young populations of galaxies with similar star formation rates compared to the Milky Way. Although this is only a lower limit the estimate is broadly consistent with the low number of observed peculiar thermonuclear supernovae.

ACKNOWLEDGMENTS

This research benefited from interactions that were funded by the Gordon and Betty Moore Foundation through grant GBMF5076. This work was supported by the National Science Foundation through grants PHY-1748958 and ACI-1663688. TK would like to thank Ylva Göteborg for providing the template for Fig. 4. TK acknowledges support from the National Science Foundation through grant AST #2107982. DS was supported by the Deutsche Forschungsgemeinschaft (DFG) under grants HE 1356/70-1 and IR 190/1-1.

Observations were obtained with the Samuel Oschin Telescope at the Palomar Observatory as part of the PTF project, a scientific collaboration between the California Institute of Technology, Columbia University, Las Cumbres Observatory, the Lawrence Berkeley National Laboratory, the National Energy Research Scientific Computing Center, the University of Oxford, and the Weizmann Institute of Science.

Based on observations obtained with the Samuel Oschin 48-inch Telescope at the Palomar Observatory as part of the Zwicky Transient Facility project. ZTF is supported by the National Science Foundation under Grant No. AST-1440341 and a collaboration including Caltech, IPAC, the Weizmann Institute for Science, the Oskar Klein Center at Stockholm University, the University of Maryland, the University of Washington, Deutsches Elektronen-Synchrotron and Humboldt University, Los Alamos National Laboratories, the TANGO Consortium of Taiwan, the University of Wisconsin at Milwaukee, and Lawrence Berkeley National Laboratories. Operations are conducted by COO, IPAC, and UW.

Some of the data presented herein were obtained at the W.M. Keck Observatory, which is operated as a scientific partnership among the California Institute of Technology, the University of California and the National Aeronautics and Space Administration. The Observatory was made possible by the generous financial support of the W.M. Keck Foundation. The authors wish to recognize and acknowledge the very significant cultural role and reverence that the summit of Mauna Kea has always had within the indigenous Hawaiian community. We are most fortunate to have the opportunity to conduct observations from this mountain.

Some results presented in this paper are based on observations made with the WHT operated on the island of La Palma by the Isaac Newton Group in the Spanish Observatorio del Roque de los Muchachos of the Instituto de Astrofísica de Canarias.

This work has made use of data from the European Space Agency (ESA) mission *Gaia* (<https://www.cosmos.esa.int/gaia>), processed by the *Gaia* Data Processing and Analysis Consortium (DPAC, <https://www.cosmos.esa.int/web/gaia/dpac/consortium>). Funding for the DPAC has been provided by national institutions, in particular the institutions participating in the *Gaia* Multilateral Agreement.

Facilities: PO:1.2m (PTF), PO:1.2m (ZTF), Hale (DBSP), ING:Herschel (ISIS), Keck:I (HIRES), Keck:II (ESI), Hale (Chimera)

Software: Gatspy (VanderPlas & Ivezić 2015; Vanderplas 2015), FITSB2 (Napiwotzki et al. 2004), LCURVE (Copperwheat et al. 2010), emcee (Foreman-Mackey et al. 2013), MESA (Paxton et al. 2011, 2013, 2015, 2018, 2019), Matplotlib

(Hunter 2007), **Astropy** (Astropy Collaboration et al. 2013, 2018), **Numpy** (Oliphant 2015), **ISIS** (Houck & Denicola 2000), **MAKEE** (<https://sites.astro.caltech.edu/~tb/makee/>)

REFERENCES

- Allen, C., & Santillan, A. 1991, *RMxAA*, 22, 255
- Astropy Collaboration, Robitaille, T. P., Tollerud, E. J., et al. 2013, *A&A*, 558, A33, doi: [10.1051/0004-6361/201322068](https://doi.org/10.1051/0004-6361/201322068)
- Astropy Collaboration, Price-Whelan, A. M., Sipőcz, B. M., et al. 2018, *AJ*, 156, 123, doi: [10.3847/1538-3881/aabc4f](https://doi.org/10.3847/1538-3881/aabc4f)
- Bauer, E. B., & Kupfer, T. 2021, *ApJ*, 922, 245, doi: [10.3847/1538-4357/ac25f0](https://doi.org/10.3847/1538-4357/ac25f0)
- Bauer, E. B., Schwab, J., & Bildsten, L. 2017, *ApJ*, 845, 97, doi: [10.3847/1538-4357/aa7ffa](https://doi.org/10.3847/1538-4357/aa7ffa)
- Bauer, E. B., White, C. J., & Bildsten, L. 2019, *ApJ*, 887, 68, doi: [10.3847/1538-4357/ab4ea4](https://doi.org/10.3847/1538-4357/ab4ea4)
- Bellm, E. C., & Sesar, B. 2016, pyraf-dbsp: Reduction pipeline for the Palomar Double Beam Spectrograph, Astrophysics Source Code Library. <http://ascl.net/1602.002>
- Bellm, E. C., Kulkarni, S. R., Graham, M. J., et al. 2019, *PASP*, 131, 018002, doi: [10.1088/1538-3873/aaecbe](https://doi.org/10.1088/1538-3873/aaecbe)
- Bildsten, L., Shen, K. J., Weinberg, N. N., & Nelemans, G. 2007, *ApJL*, 662, L95, doi: [10.1086/519489](https://doi.org/10.1086/519489)
- Bloemen, S., Marsh, T. R., Østensen, R. H., et al. 2011, *MNRAS*, 410, 1787, doi: [10.1111/j.1365-2966.2010.17559.x](https://doi.org/10.1111/j.1365-2966.2010.17559.x)
- Brooks, J., Bildsten, L., Marchant, P., & Paxton, B. 2015, *ApJ*, 807, 74, doi: [10.1088/0004-637X/807/1/74](https://doi.org/10.1088/0004-637X/807/1/74)
- Carter, D., et al. 1993
- Chambers, K. C., Magnier, E. A., Metcalfe, N., et al. 2016, arXiv e-prints. <https://arxiv.org/abs/1612.05560>
- Choi, J., Dotter, A., Conroy, C., et al. 2016, *ApJ*, 823, 102, doi: [10.3847/0004-637X/823/2/102](https://doi.org/10.3847/0004-637X/823/2/102)
- Claret, A., & Bloemen, S. 2011, *A&A*, 529, A75, doi: [10.1051/0004-6361/201116451](https://doi.org/10.1051/0004-6361/201116451)
- Copperwheat, C. M., Marsh, T. R., Dhillon, V. S., et al. 2010, *MNRAS*, 402, 1824, doi: [10.1111/j.1365-2966.2009.16010.x](https://doi.org/10.1111/j.1365-2966.2009.16010.x)
- Cummings, J. D., Kalirai, J. S., Tremblay, P. E., Ramirez-Ruiz, E., & Choi, J. 2018, *ApJ*, 866, 21, doi: [10.3847/1538-4357/aadfd6](https://doi.org/10.3847/1538-4357/aadfd6)
- De, K., Kasliwal, M. M., Polin, A., et al. 2019, *ApJL*, 873, L18, doi: [10.3847/2041-8213/ab0aec](https://doi.org/10.3847/2041-8213/ab0aec)
- De, K., Kasliwal, M. M., Tzanidakis, A., et al. 2020, *ApJ*, 905, 58, doi: [10.3847/1538-4357/abb45c](https://doi.org/10.3847/1538-4357/abb45c)
- Dhillon, V. S., Marsh, T. R., Stevenson, M. J., et al. 2007, *MNRAS*, 378, 825, doi: [10.1111/j.1365-2966.2007.11881.x](https://doi.org/10.1111/j.1365-2966.2007.11881.x)
- Dotter, A. 2016, *ApJS*, 222, 8, doi: [10.3847/0067-0049/222/1/8](https://doi.org/10.3847/0067-0049/222/1/8)
- Fink, M., Röpke, F. K., Hillebrandt, W., et al. 2010, *A&A*, 514, A53, doi: [10.1051/0004-6361/200913892](https://doi.org/10.1051/0004-6361/200913892)
- Foreman-Mackey, D., Hogg, D. W., Lang, D., & Goodman, J. 2013, *PASP*, 125, 306, doi: [10.1086/670067](https://doi.org/10.1086/670067)
- Gaia Collaboration, Prusti, T., de Bruijne, J. H. J., et al. 2016, *A&A*, 595, A1, doi: [10.1051/0004-6361/201629272](https://doi.org/10.1051/0004-6361/201629272)
- Gaia Collaboration, Brown, A. G. A., Vallenari, A., et al. 2018, *A&A*, 616, A1, doi: [10.1051/0004-6361/201833051](https://doi.org/10.1051/0004-6361/201833051)
- . 2021, *A&A*, 649, A1, doi: [10.1051/0004-6361/202039657](https://doi.org/10.1051/0004-6361/202039657)
- Geier, S., Raddi, R., Gentile Fusillo, N. P., & Marsh, T. R. 2019, *A&A*, 621, A38, doi: [10.1051/0004-6361/201834236](https://doi.org/10.1051/0004-6361/201834236)
- Geier, S., Hirsch, H., Tillich, A., et al. 2011, *A&A*, 530, A28, doi: [10.1051/0004-6361/201015316](https://doi.org/10.1051/0004-6361/201015316)
- Geier, S., Marsh, T. R., Wang, B., et al. 2013, *A&A*, 554, A54, doi: [10.1051/0004-6361/201321395](https://doi.org/10.1051/0004-6361/201321395)
- Graham, M. J., Kulkarni, S. R., Bellm, E. C., et al. 2019, arXiv e-prints. <https://arxiv.org/abs/1902.01945>
- Green, G. M., Schlafly, E., Zucker, C., Speagle, J. S., & Finkbeiner, D. 2019, *ApJ*, 887, 93, doi: [10.3847/1538-4357/ab5362](https://doi.org/10.3847/1538-4357/ab5362)
- Han, Z., Podsiadlowski, P., Maxted, P. F. L., & Marsh, T. R. 2003, *MNRAS*, 341, 669, doi: [10.1046/j.1365-8711.2003.06451.x](https://doi.org/10.1046/j.1365-8711.2003.06451.x)
- Han, Z., Podsiadlowski, P., Maxted, P. F. L., Marsh, T. R., & Ivanova, N. 2002, *MNRAS*, 336, 449, doi: [10.1046/j.1365-8711.2002.05752.x](https://doi.org/10.1046/j.1365-8711.2002.05752.x)
- Harding, L. K., Hallinan, G., Milburn, J., et al. 2016, *MNRAS*, 457, 3036, doi: [10.1093/mnras/stw094](https://doi.org/10.1093/mnras/stw094)
- Heber, U. 1986, *A&A*, 155, 33
- . 2009, *ARA&A*, 47, 211, doi: [10.1146/annurev-astro-082708-101836](https://doi.org/10.1146/annurev-astro-082708-101836)
- . 2016, *PASP*, 128, 082001, doi: [10.1088/1538-3873/128/966/082001](https://doi.org/10.1088/1538-3873/128/966/082001)
- Heber, U., Reid, I. N., & Werner, K. 2000, *A&A*, 363, 198
- Houck, J. C., & Denicola, L. A. 2000, in *Astronomical Society of the Pacific Conference Series*, Vol. 216, *Astronomical Data Analysis Software and Systems IX*, ed. N. Manset, C. Veillet, & D. Crabtree, 591
- Hunter, J. D. 2007, *Computing In Science & Engineering*, 9, 90, doi: [10.1109/MCSE.2007.55](https://doi.org/10.1109/MCSE.2007.55)
- Iben, Jr., I., & Tutukov, A. V. 1991, *ApJ*, 370, 615, doi: [10.1086/169848](https://doi.org/10.1086/169848)

- Irrgang, A., Wilcox, B., Tucker, E., & Schiefelbein, L. 2013, *A&A*, 549, A137, doi: [10.1051/0004-6361/201220540](https://doi.org/10.1051/0004-6361/201220540)
- Kupfer, T., Geier, S., Heber, U., et al. 2015, *A&A*, 576, A44, doi: [10.1051/0004-6361/201425213](https://doi.org/10.1051/0004-6361/201425213)
- Kupfer, T., van Roestel, J., Brooks, J., et al. 2017a, *ApJ*, 835, 131, doi: [10.3847/1538-4357/835/2/131](https://doi.org/10.3847/1538-4357/835/2/131)
- Kupfer, T., Ramsay, G., van Roestel, J., et al. 2017b, *ApJ*, 851, 28, doi: [10.3847/1538-4357/aa9522](https://doi.org/10.3847/1538-4357/aa9522)
- Kupfer, T., Bauer, E. B., Marsh, T. R., et al. 2020a, *ApJ*, 891, 45, doi: [10.3847/1538-4357/ab72ff](https://doi.org/10.3847/1538-4357/ab72ff)
- Kupfer, T., Bauer, E. B., Burdge, K. B., et al. 2020b, *ApJL*, 898, L25, doi: [10.3847/2041-8213/aba3c2](https://doi.org/10.3847/2041-8213/aba3c2)
- Kupfer, T., Prince, T. A., van Roestel, J., et al. 2021, *MNRAS*, 505, 1254, doi: [10.1093/mnras/stab1344](https://doi.org/10.1093/mnras/stab1344)
- Laher, R. R., Surace, J., Grillmair, C. J., et al. 2014, *PASP*, 126, 674, doi: [10.1086/677351](https://doi.org/10.1086/677351)
- Law, N. M., Kulkarni, S. R., Dekany, R. G., et al. 2009, *PASP*, 121, 1395, doi: [10.1086/648598](https://doi.org/10.1086/648598)
- Liu, Z.-W., Röpkke, F. K., Zeng, Y., & Heger, A. 2021, *A&A*, 654, A103, doi: [10.1051/0004-6361/202141518](https://doi.org/10.1051/0004-6361/202141518)
- Livne, E. 1990, *ApJL*, 354, L53, doi: [10.1086/185721](https://doi.org/10.1086/185721)
- Livne, E., & Arnett, D. 1995, *ApJ*, 452, 62, doi: [10.1086/176279](https://doi.org/10.1086/176279)
- Masci, F. J., Laher, R. R., Rusholme, B., et al. 2019, *PASP*, 131, 018003, doi: [10.1088/1538-3873/aae8ac](https://doi.org/10.1088/1538-3873/aae8ac)
- Maxted, P. f. L., Heber, U., Marsh, T. R., & North, R. C. 2001, *MNRAS*, 326, 1391, doi: [10.1111/j.1365-8711.2001.04714.x](https://doi.org/10.1111/j.1365-8711.2001.04714.x)
- Napiwotzki, R., Karl, C. A., Lisker, T., et al. 2004, *Astrophysics and Space Science*, 291, 321, doi: [10.1023/B:ASTR.0000044362.07416.6c](https://doi.org/10.1023/B:ASTR.0000044362.07416.6c)
- Nelemans, G. 2010, *Ap&SS*, 329, 25, doi: [10.1007/s10509-010-0392-0](https://doi.org/10.1007/s10509-010-0392-0)
- Neunteufel, P. 2020, *A&A*, 641, A52, doi: [10.1051/0004-6361/202037792](https://doi.org/10.1051/0004-6361/202037792)
- Neunteufel, P., Kruckow, M., Geier, S., & Hamers, A. S. 2021, *A&A*, 646, L8, doi: [10.1051/0004-6361/202040022](https://doi.org/10.1051/0004-6361/202040022)
- Neunteufel, P., Yoon, S. C., & Langer, N. 2019, *A&A*, 627, A14, doi: [10.1051/0004-6361/201935322](https://doi.org/10.1051/0004-6361/201935322)
- Odenkirchen, M., & Brosche, P. 1992, *Astronomische Nachrichten*, 313, 69, doi: [10.1002/asna.2113130204](https://doi.org/10.1002/asna.2113130204)
- Ofek, E. O., Laher, R., Law, N., et al. 2012, *PASP*, 124, 62, doi: [10.1086/664065](https://doi.org/10.1086/664065)
- Oke, J. B., & Gunn, J. E. 1982, *PASP*, 94, 586, doi: [10.1086/131027](https://doi.org/10.1086/131027)
- Oliphant, T. E. 2015, *Guide to NumPy*, 2nd edn. (USA: CreateSpace Independent Publishing Platform)
- Ostrowski, J., Baran, A. S., Sanjayan, S., & Sahoo, S. K. 2021, *MNRAS*, 503, 4646, doi: [10.1093/mnras/staa3751](https://doi.org/10.1093/mnras/staa3751)
- Pauli, E.-M., Napiwotzki, R., Heber, U., Altmann, M., & Odenkirchen, M. 2006, *A&A*, 447, 173, doi: [10.1051/0004-6361:20052730](https://doi.org/10.1051/0004-6361:20052730)
- Paxton, B., Bildsten, L., Dotter, A., et al. 2011, *ApJs*, 192, 3, doi: [10.1088/0067-0049/192/1/3](https://doi.org/10.1088/0067-0049/192/1/3)
- Paxton, B., Cantiello, M., Arras, P., et al. 2013, *ApJs*, 208, 4, doi: [10.1088/0067-0049/208/1/4](https://doi.org/10.1088/0067-0049/208/1/4)
- Paxton, B., Marchant, P., Schwab, J., et al. 2015, *ApJs*, 220, 15, doi: [10.1088/0067-0049/220/1/15](https://doi.org/10.1088/0067-0049/220/1/15)
- Paxton, B., Schwab, J., Bauer, E. B., et al. 2018, *ApJS*, 234, 34, doi: [10.3847/1538-4365/aaa5a8](https://doi.org/10.3847/1538-4365/aaa5a8)
- Paxton, B., Smolec, R., Schwab, J., et al. 2019, *ApJS*, 243, 10, doi: [10.3847/1538-4365/ab2241](https://doi.org/10.3847/1538-4365/ab2241)
- Pelisoli, I., Neunteufel, P., Geier, S., et al. 2021, *Nature Astronomy*, 5, 1052, doi: [10.1038/s41550-021-01413-0](https://doi.org/10.1038/s41550-021-01413-0)
- Piersanti, L., Tornambé, A., & Yungelson, L. R. 2014, *MNRAS*, 445, 3239, doi: [10.1093/mnras/stu1885](https://doi.org/10.1093/mnras/stu1885)
- Polin, A., Nugent, P., & Kasen, D. 2019, *ApJ*, 873, 84, doi: [10.3847/1538-4357/aafb6a](https://doi.org/10.3847/1538-4357/aafb6a)
- . 2021, *ApJ*, 906, 65, doi: [10.3847/1538-4357/abccccc](https://doi.org/10.3847/1538-4357/abccccc)
- Preece, H. P., Tout, C. A., & Jeffery, C. S. 2018, *MNRAS*, 481, 715, doi: [10.1093/mnras/sty2091](https://doi.org/10.1093/mnras/sty2091)
- Ratzloff, J. K., Barlow, B. N., Kupfer, T., et al. 2019, *ApJ*, 883, 51, doi: [10.3847/1538-4357/ab3727](https://doi.org/10.3847/1538-4357/ab3727)
- Rau, A., Kulkarni, S. R., Law, N. M., et al. 2009, *PASP*, 121, 1334, doi: [10.1086/605911](https://doi.org/10.1086/605911)
- Romero, A. D., Kepler, S. O., Joyce, S. R. G., Lauffer, G. R., & Córscico, A. H. 2019, *MNRAS*, 484, 2711, doi: [10.1093/mnras/stz160](https://doi.org/10.1093/mnras/stz160)
- Ruiter, A. J., Belczynski, K., Benacquista, M., Larson, S. L., & Williams, G. 2010, *ApJ*, 717, 1006, doi: [10.1088/0004-637X/717/2/1006](https://doi.org/10.1088/0004-637X/717/2/1006)
- Savonije, G. J., de Kool, M., & van den Heuvel, E. P. J. 1986, *A&A*, 155, 51
- Shen, K. J., & Bildsten, L. 2014, *ApJ*, 785, 61, doi: [10.1088/0004-637X/785/1/61](https://doi.org/10.1088/0004-637X/785/1/61)
- Sullivan, M., Le Borgne, D., Pritchett, C. J., et al. 2006, *ApJ*, 648, 868, doi: [10.1086/506137](https://doi.org/10.1086/506137)
- Tutukov, A. V., & Fedorova, A. V. 1989, *Soviet Astronomy*, 33, 606
- Tutukov, A. V., & Yungelson, L. R. 1990, *Soviet Ast.*, 34, 57
- Vanderplas, J. 2015, *gatspy: General tools for Astronomical Time Series in Python*, v0.3.0, Zenodo, doi: [10.5281/zenodo.14833](https://doi.org/10.5281/zenodo.14833)
- VanderPlas, J. T., & Ivezić, v. 2015, *ApJ*, 812, 18, doi: [10.1088/0004-637X/812/1/18](https://doi.org/10.1088/0004-637X/812/1/18)
- Vennes, S., Kawka, A., O’Toole, S. J., Németh, P., & Burton, D. 2012, *ApJL*, 759, L25, doi: [10.1088/2041-8205/759/1/L25](https://doi.org/10.1088/2041-8205/759/1/L25)

- Wang, B. 2018, ArXiv e-prints.
<https://arxiv.org/abs/1801.04031>
- Wang, B., & Han, Z. 2012, *NewAR*, 56, 122,
doi: [10.1016/j.newar.2012.04.001](https://doi.org/10.1016/j.newar.2012.04.001)
- Woosley, S. E., & Kasen, D. 2011, *ApJ*, 734, 38,
doi: [10.1088/0004-637X/734/1/38](https://doi.org/10.1088/0004-637X/734/1/38)
- Woosley, S. E., & Weaver, T. A. 1994, *ApJ*, 423, 371,
doi: [10.1086/173813](https://doi.org/10.1086/173813)
- Yungelson, L. R. 2008, *Astronomy Letters*, 34, 620,
doi: [10.1134/S1063773708090053](https://doi.org/10.1134/S1063773708090053)
- Zahn, J.-P. 1977, *A&A*, 57, 383